GEOFIZIKA VOL. 30 2013

Original scientific paper
UDC 550.34.013

Study of combined effects of sediment rheology and anticlinal basement topography on ground motion characteristics

Vinay Kumar and J. P. Narayan

Indian Institute of Technology Roorkee, Department of Earthquake Engineering, Roorkee, India

Received 7 November 2012, in final form 28 March 2013

A very peculiar damage patterns have been reported during Northridge earthquake of 1994 and Nisqually earthquake of 2001 caused by basement focusing. Similarly, basement de-focusing may cause lesser damage than the expectations but such inferences have not been reported. Further, as far as we know, no theoretical study related to de-focusing effects of anticlinal basement topography (ABT) is available in the literature. In order to fulfill this gap, this article presents the combined effects of sediment rheology and ABT on the SH- and SV-waves characteristics. The simulated results revealed an increase of de-amplification factors with distance travelled in basin above the ABT. The computed snapshots also confirmed amplitude de-amplification, diffraction and mode conversion of SV-wave. Elastic response revealed that the de-amplification factors caused by ABT were not frequency dependent. The average spectral de-amplification factors were more or less same for both the waves even after strong mode conversion of SV-wave at the lower part of ABT. Based on simulated results, it was inferred that the incorporation of effects of ABT in seismic hazard assessment is equally important as that of synclinal basement topography (SBT) effects for cost effective earthquake engineering.

Keywords: simulation of viscoelastic seismic response, finite difference method, mode conversion, basement topography effects and local site effects

1. Introduction

The observed damage patterns during past earthquakes reveal significant differences in structural damage in a basin as compared with the surrounding exposed rocks, or even in the basin itself from place to place (Narayan, 2005, 2012). Sometimes very peculiar damage pattern is observed, which cannot be explained based on the soil amplification or soil resonance effects in basin as was observed in Santa Monica, Los Angeles basin during Northridge earthquake of 1994 due to the basement focusing effects (Gao et al., 1996; Alex and Olsen, 1998; Davis et al., 2000). Similarly, the shallow basement focusing effects during 1949

Olympia earthquake ($M = 7.1$), 1965 Tacoma earthquake ($M = 6.5$) and 2001 Nisqually earthquake ($M = 6.8$) caused consistently anomalous damage to unreinforced brick chimneys in west Seattle, Washington (Booth et al., 2004; Stephenson et al., 2006). It is also important to quantify the effects of basement de-focusing to infer the level of de-amplification caused by ABT for seismic hazard assessment and cost effective earthquake engineering.

Realistic quantification of local site effects, like basement topography, on the ground motion characteristics requires an efficient numerical method. The staggered grid fourth order accurate finite-difference (FD) method, proposed by Madariaga (1976), is one of the most useful numerical methods to simulate the ground motion characteristics (Levander, 1988; Moczo et al., 2002; Narayan and Kumar, 2008, 2010; Narayan and Kumar, 2012, 2013). The explicit staggered grid FD has been used successfully to simulate the scattering and diffraction phenomenon at the basin edges, underground ridges and surface topography as well as the role of these phenomenons in surface wave generation as per physics (Virieux, 1986; Moczo et al., 1993; Narayan and Rao, 2003; Narayan, 2003; Narayan and Ram, 2006). The accuracy of time domain FD method very much depends on the implementation of realistic viscoelastic damping in simulation. Day and Minster (1984) first time attempted to incorporate the viscoelastic damping into a 2D time-domain FD algorithm based on Padé approximation. Emmerich and Korn (1987) improved the incorporation of viscoelastic damping in time domain simulation using generalized Maxwell body rheological model (widely known as GMB-EK model). Kristek and Moczo (2003) introduced material independent anelastic function which is better one in case of material discontinuity in the FD grid.

The combined effects of sediment damping and anticlinal basement topography (ABT) on ground motion characteristics are studied in details. Davis et al. (2000) reported that elastic basement focusing causes frequency dependent amplification. One of the aims of this paper is to infer whether de-amplification caused by ABT is frequency dependent or not. Fourth order staggered grid finite-difference SH-wave and P-SV wave algorithms have been used for the simulation of viscoelastic seismic responses of considered ABT models. In order to separate the ABT de-amplification effects from the free surface effects (layer resonance, etc.), unbounded model is considered. However, realistic scenario including both the ABT de-focusing and free surface effects should be simulated to provide a useful input for the earthquake engineering purposes, instead of a simple models used here purposely. Both the in plane and out of plane seismic responses of an unbounded ABT model on a vertical array along the axis of ABT are simulated for different sediment damping. The spectral de-amplification caused by ABT and the effect of soil damping is computed just by taking the spectral ratio of responses with and without ABT in the respective considered models. Snapshots at different times are also computed for the identification of different seismic phases caused by ABT structure.

2. Salient features of the used FD programs

In order to accurately simulate the effects of ABT on ground motion characteristics, (2,4) staggered-grid SH-wave and P-SV wave FD algorithms recently developed by Narayan and Kumar (2012, 2013) were used. These algorithms are

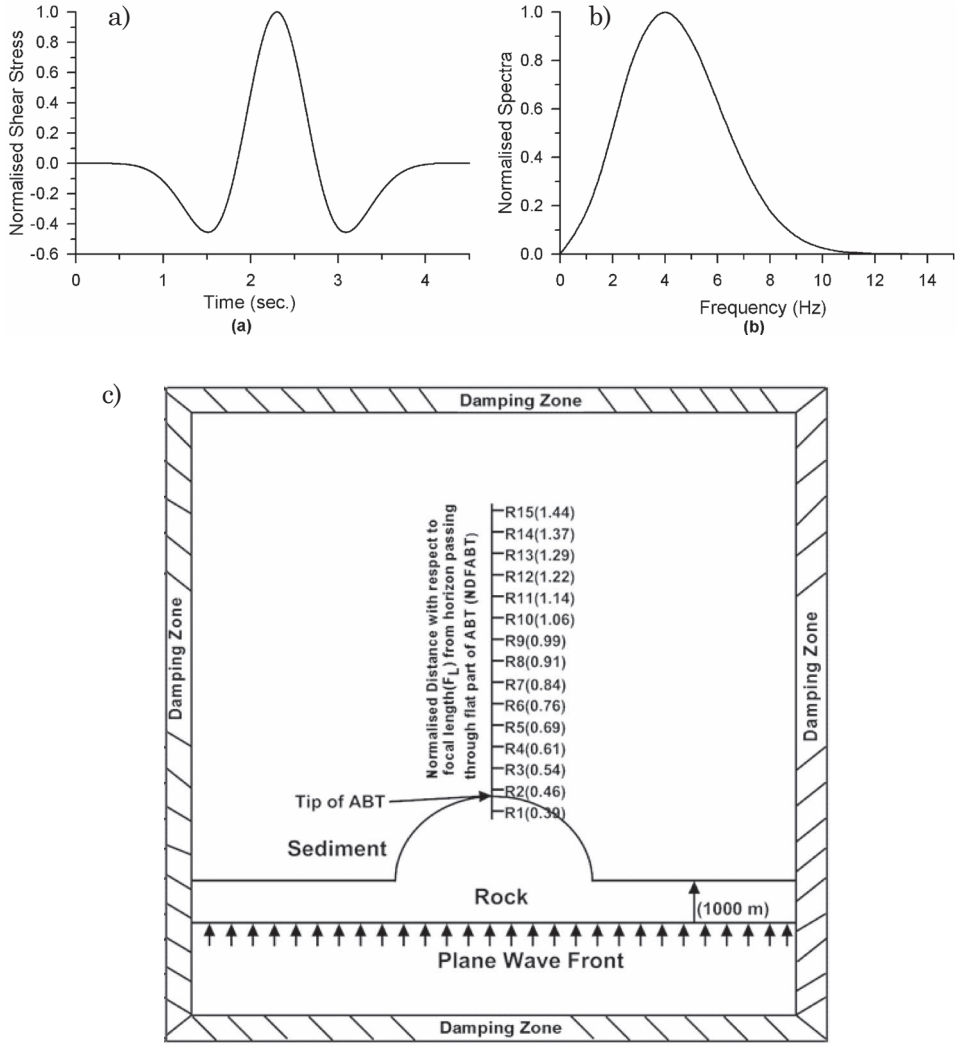

Figure 1. The normalized Ricker wavelet (a) and its spectra (b) with 4.0 Hz dominant frequency and anticlinal basement topography (ABT) model with a vertical array passing along the focal length of ABT (c) (The distance of receiver points from the horizontal part of ABT is normalised with the focal length (F_L) of ABT and referred as NDFABT in the manuscript).

based on FD approximation of velocity-stress viscoelastodynamic SH-wave and P-SV wave equations for heterogeneous medium. The incorporation of realistic damping in these FD algorithms is based on a GMB-EK rheological model (Kristek and Moczo, 2003). Both the sponge boundary (Israeli and Orszag, 1981) and absorbing boundary condition of Clayton and Engquist (1977) were implemented on the model edges to avoid the edge reflections (Kumar and Narayan, 2008). The four stress relaxation frequencies used in the computations were taken as 0.02 Hz, 0.2 Hz, 2.0 Hz and 20 Hz. A Ricker wavelet used as a source excitation function was generated with the help of a second derivative of convolution of a Gaussian function ($H = \exp[-\alpha(T-T_0)^2]$) and a polynomial window ($G = [1-(\tau-1)^2]^3$). Where $\alpha = (\pi F_0)^2$, F_0 is dominant frequency, $\tau = T / T_0$, T_0 is dominant period and T is the duration of the wavelet (Narayan, 2005). Fig. 1 shows the generated Ricker wavelet and its spectra with dominant frequency 4 Hz and upper cutoff frequency 10 Hz. A horizontal plane wave front for SH-wave or SV-wave was generated into the numerical grid using various point sources at a particular horizon keeping five point sources per- dominant wavelength, as shown in Fig. 1c.

3. Effects of rheology and ABT on SH-wave

In order to study the combined effects of ABT and sediment rheology on the ground motion characteristics, an unbounded ABT model consisting of single sedimentary layer with different rheology above the ABT is considered. Figure 1c shows the north-south cross-section of ABT model which is elongated in east-west direction. The vertical distances are measured with respect to the horizon passing through base of ABT and horizontal distances are measured with respect to the axis of ABT. The positive x-coordinate was pointing towards north and positive z-coordinate was pointing upward. The shape of considered ABT is half-circular and radius of curvature was taken as 3000 m. The S-wave and P-wave velocities and quality factors at reference frequency, density and unrelaxed moduli of sedimentary deposit and basement rock are given in Tab. 1 for different rheological models for sediment (ABTM1-ABTM4). A plane S-wave front was generated at a depth of 1000 m below the base of ABT. Seismic responses were computed at 15 equidistant (500 m apart) receiver points on a vertical array extending from 450 m below the tip of ABT to 6550 m above the same.

Seismic responses of both the elastic (ABTM1) and viscoelastic (ABTM2-ABTM4) models were computed. In order to separate out the combined effects of ABT de-focusing and sediment damping from the impedance contrast (IC), seismic responses without ABT were computed keeping the position of horizontal interface between sediment and the basement rock at the tip of the ABT. Further, there is no divergence effect in the simulation since horizontal plane wave fronts of SH-wave and SV-waves are being used in the simulations. So, the response computed on a vertical array just above the interface between the sediment and bedrock may be used for assessing the ABT de-focusing and sediment effects on receiver points above the ABT.

3.1. SH-wave seismic response

The simulated SH-wave seismic response of elastic ABTM1 model on a vertical array along the axis of ABT is shown in Fig. 2. The distance of receiver

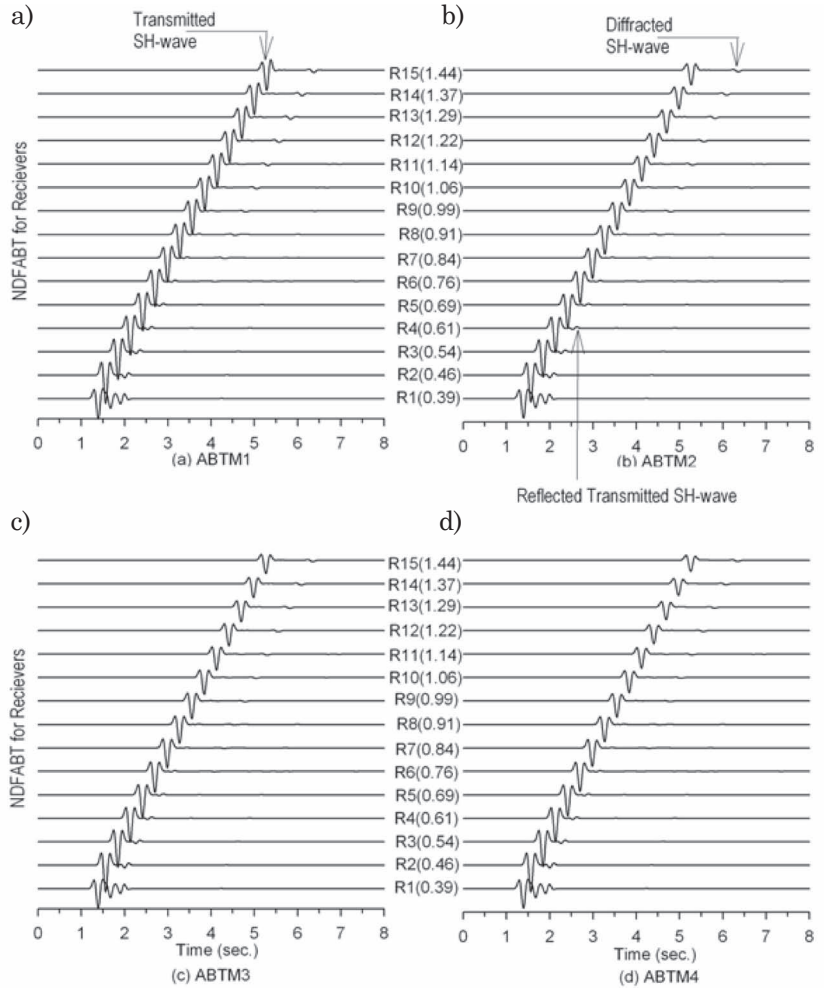

Figure 2. SH-wave seismic responses of ABT models on a vertical array (Note: The numerical value in the bracket denotes the NDFABT value of receiver point).

points from the horizontal part of ABT is normalised with the focal length (F_L) of ABT and referred as NDFABT in the manuscript. The focal length (F_L) of ABT was computed using the following equation

Table 1. Rheological parameters for sedimentary deposit above basement for different basement topography models (ABTM1-ABTM4).

	SBT models	Velocity at F_R (m/sec)		Density (kg/m^3)	Quality factor at F_R		Unrelaxed moduli (GPa)		
		S-wave	P-wave		S-wave	P-wave	M_U	K_U	λ_U
Sediment deposits	ABTM1	1750	3031	2200	---	---	6.737	20.212	6.737
	ABTM2	1750	3031	2200	175	303	6.851	20.407	6.704
	ABTM3	1750	3031	2200	131	227	6.889	20.473	6.693
	ABTM4	1750	3031	2200	85	151	6.967	20.605	6.670
Basement rock	ABTM1	3200	5542	2800	---	---	28.672	86.016	28.672
	ABTM2	3200	5542	2800	320	554	28.935	86.453	28.582
	ABTM3	3200	5542	2800	320	554	28.935	86.453	28.582
	ABTM4	3200	5542	2800	320	554	28.935	86.453	28.582

$$F_L = \frac{r}{(1-\eta)}$$

where r is the radius of circular ABT and η is the ratio of S-wave velocity in sediment to that in basement rock. An analysis of Fig. 2a depicts that there is decrease of amplitude of transmitted SH-wave with increase of distance travelled in basin due to ABT de-focusing effect. The reflected-transmitted waves are the second arrivals and the direct-diffracted waves from the corners of the ABT are the third arrivals. The waves reflected from the inner part of ABT in upwards direction and then transmitted in to the sediment are referred as „reflected transmitted waves" in the manuscript. The amplitudes of direct-diffracted waves are highly variable. The receiver R1 located in basement depicts both the up-going SH-wave and the reflected SH-wave from the ABT.

Similarly, Figs. 2b–2d show the responses of viscoelastic ABTM2-ABTM4 models, respectively. The analysis of Fig. 2 reveals the ABT de-focusing effects along with the effects of change of rheology of sediments on the ground motion characteristics. The effect of rheology is very much clearly visible on the decrease of amplitudes of transmitted SH-wave, reflected-transmitted and direct-diffracted SH-waves in accordance with the sediment damping.

3.2. SH-wave snapshots

In order to further demonstrate the ABT de-focusing effects on the transmitted SH-waves and development of reflected-transmitted waves and diffractions from the corners of ABT, snapshots were computed at different times. Snapshots were computed in a rectangular area extending from 500 m below to 9500 m above the base of ABT and 5000 m south to 5000 m north of axis of ABT. The snapshot at time 0.2 sec (Fig. 3a), depicts that SH-wave front has not entered in the considered rectangular area. Fig. 3b shows the SH-wave entered into the anticlinal part of ABT, direct-diffracted waves from the corners of ABT and transmitting SH-wave in basin along the horizontal flanks of the ABT. The focusing of reflected SH-wave from the curved part of ABT and splitting of main SH-wave front can be inferred in snapshot at time 2.0 sec (Fig. 3c).

The reflected-transmitted SH-wave in sediment along with main SH-wave front transmitted in the basin can be seen in snapshot at time 3.0 sec (Fig. 3d). The snapshots at times 4.0 and 5.0 sec depict reflected-transmitted wave in basin, direct-diffracted SH-waves, reflected-diffracted waves (wave reflected from the inner part of ABT and then diffracted at the corners of the ABT) and the reflected-transmitted-reflected waves (wave reflected from inner part of ABT, transmitted in basin and then reflected from the horizontal base of the ABT) from the horizontal flanks of the ABT very clearly. Finally, the analysis of Fig. 3 reveals the decrease of amplitude of transmitted SH-wave in basin due to the ABT defocusing.

3.3. SH-wave spectral de-amplification

In order to quantify the combined effects of sediment rheology and ABT de-focusing on the ground motion characteristics, de-amplification factors were computed in two frequency range. The spectral de-amplification was computed with respect to the trace recorded on R2 in response of model without ABT (sediment-rock interface was considered at the tip of ABT in the without ABT model). The spectral de-amplifications at different normalized distances in a low frequency range (0–0.6 Hz) are shown in Fig. 4. This figure depicts an anomalous de-amplification at 0.3 Hz. This frequency is matching with the frequency computed using sediment velocity and wavelength equal to the width of base of the ABT. Further, the spectral de-amplification at 0.3 Hz is largest in elastic ABTM1 model and decreasing with the increase of sediment damping, which seems to be an anomalous phenomenon. The decrease of deamplification at 0.3 Hz with increase of sediment damping may be due to the increase of velocity with the increase of sediment damping for the considered sediment rheology. The de-amplification factor is maximum at NDFABT 1.22 and it is systemically the decreasing with decrease of NDFABT. So, it may be concluded that certain frequency may get anomalously very large de-amplification due to ABT de-focusing, depending on radius of curvature, sediment damping and sediment velocity.

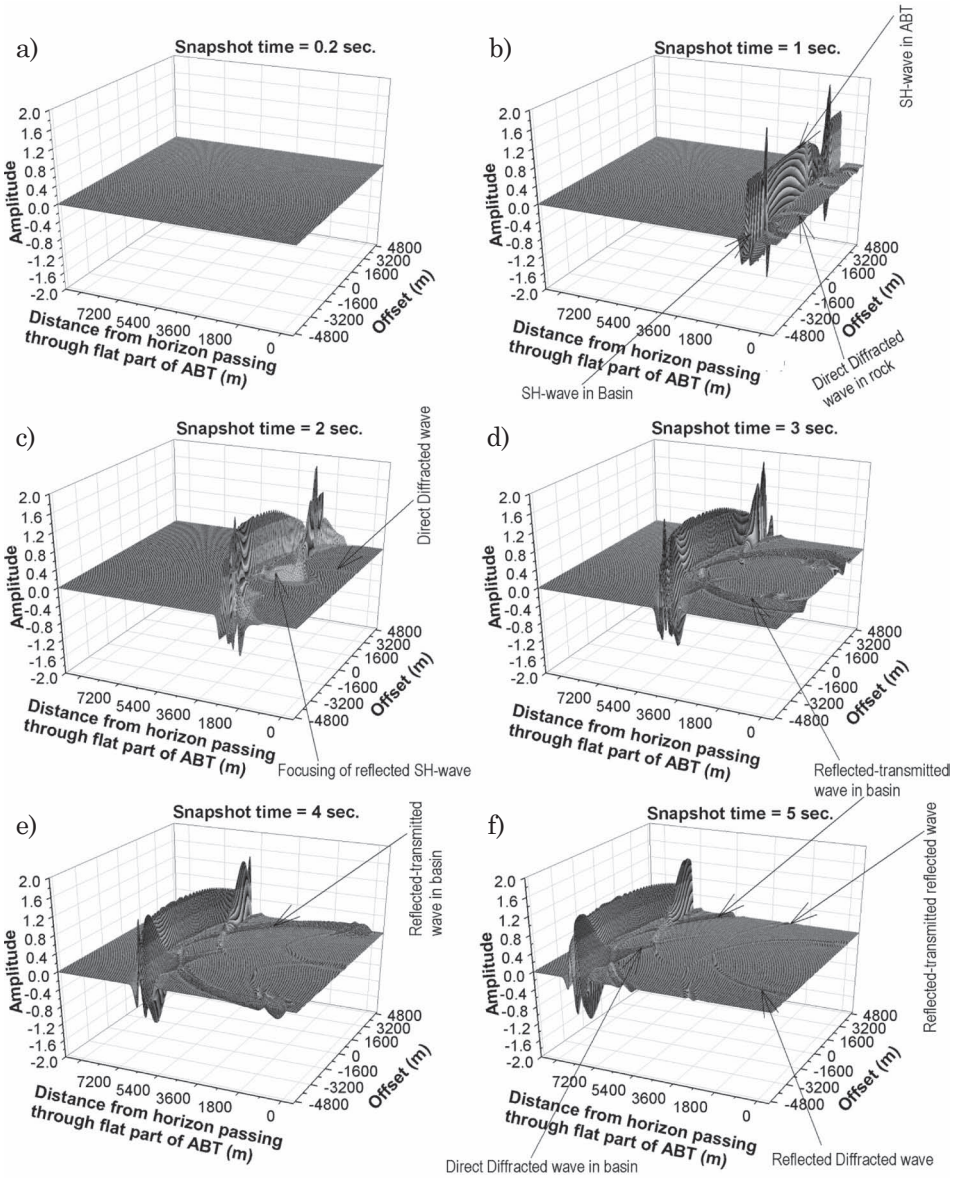

Figure 3. Snapshots of SH-wave propagation in a rectangular area at different times.

Similarly, Fig. 5 shows the spectral de-amplifications in high frequency range (0.6–10.0 Hz) at different NDFABT positions. Fig. 5a shows the spectral de-amplification factors in case of elastic ABTM1 model. Analysis of this figure

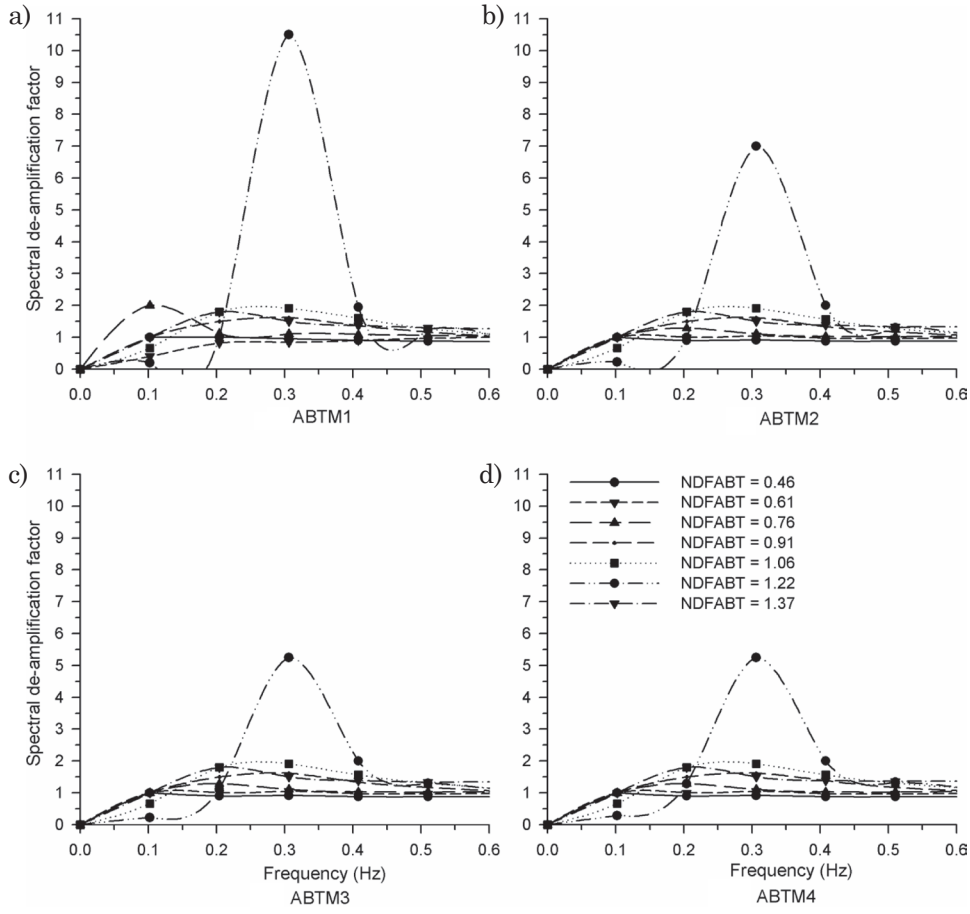

Figure 4. Spectral de-amplification factor at different NDFABT values caused by ABT de-focusing in a frequency range 0 Hz–0.6 Hz.

depicts an increase of spectral de-amplification factors with increase of NDFABT values. It can also be inferred that de-amplification factors are almost independent of frequency. This finding is in contrast to the basement focusing which causes frequency dependent amplification (Davis et al., 2000). The combined effects of ABT de-focusing and the sediment rheology on the spectral de-amplifications are shown in Figs. 5b–d. An increase of spectral de-amplification factors with the increase of sediment damping can be inferred. Further, higher frequencies are more damped due to sediment damping. The diffracted waves are affecting the spectral de-amplification factors to some extent.

The computed amplitude de-amplification factor in time domain at different NDFABT positions is shown in Fig. 6a. It was computed just by taking the ratio

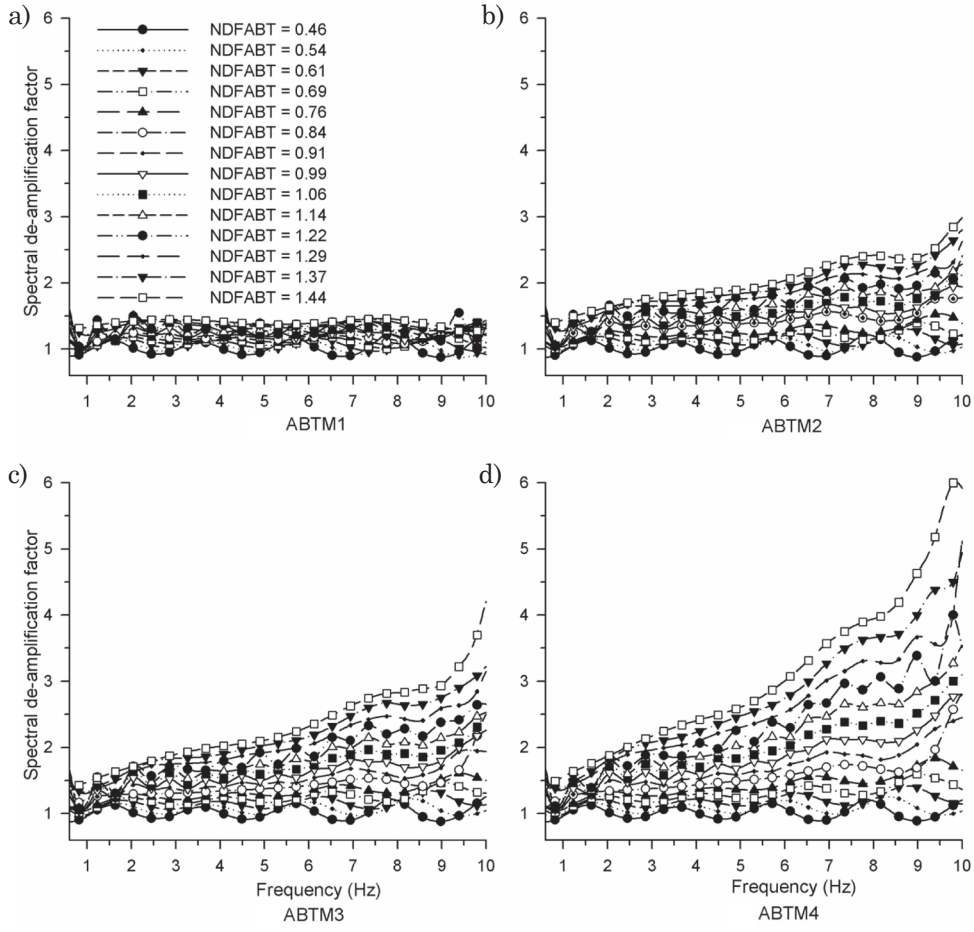

Figure 5. Spectral de-amplification factor at different NDFABT values caused by ABT de-focusing in a frequency range 0.6 Hz–10Hz.

of the maximum amplitude in the second trace of response of model without ABT in the model with maximum amplitude at different NDFABT positions with ABT in the model. There is an increase of amplitude de-amplification factor with the increase of NDFABT value. The average spectral de-amplification factors in the considered frequency range were also computed at different NDFABT positions (Fig. 6b). There is an increase of average spectral de-amplification factor with the increase of NDFABT value and decrease of sediment damping. Analysis of Fig. 6 depicts that amplitude de-amplification factor is very much similar to the average spectral de-amplification factor, but it is larger in later one.

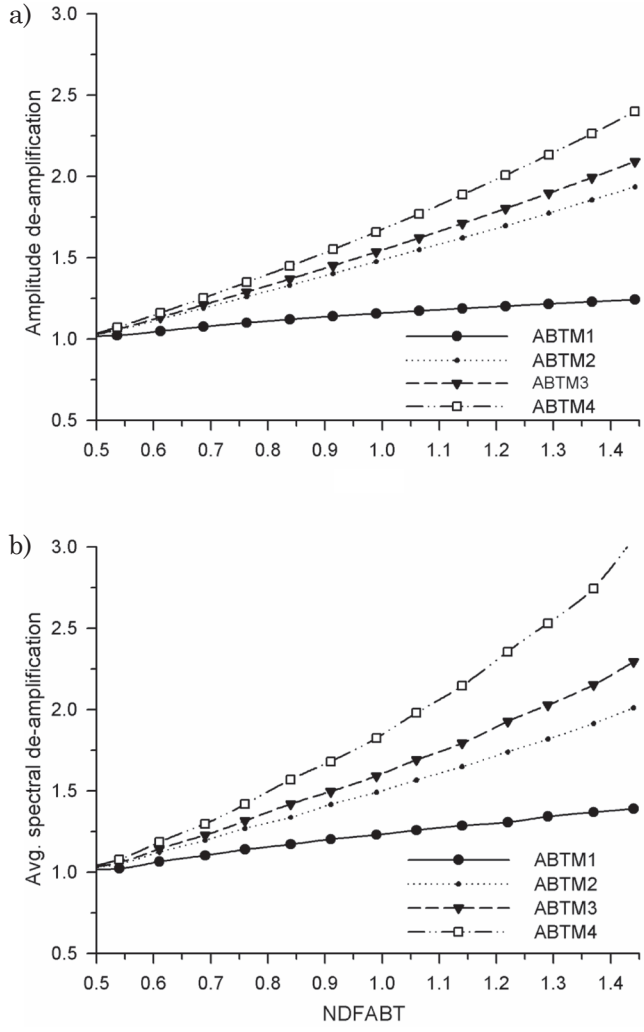

Figure 6. Amplitude de-amplification factor (a) and average spectral de-amplification factor at different NDFABT values (b).

4. Effects of rheology and ABT on P-SV wave

In order to study the combined effects of rheology of sediment and ABT on the SV-wave (in plane motion), seismic responses were computed using the same ABT model parameters (Tab. 4) and source-receiver positions (Fig. 1c).

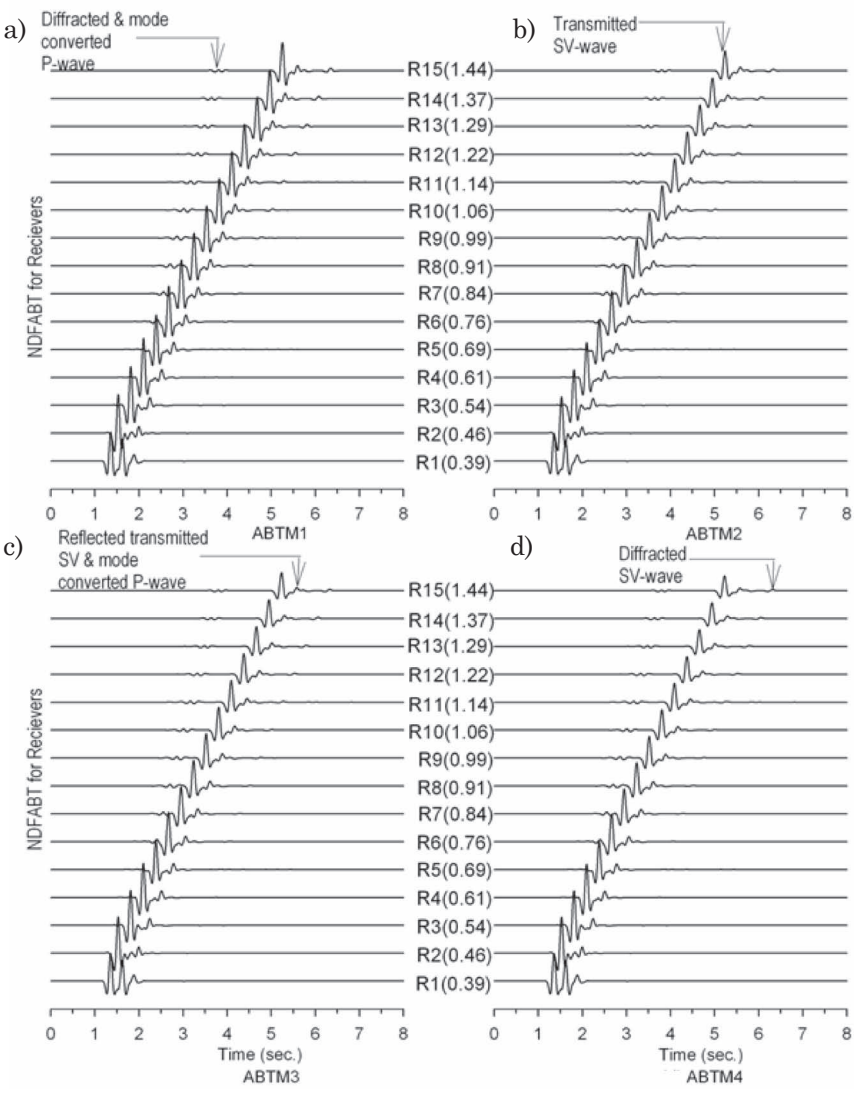

Figure 7. Horizontal component of SV-wave seismic responses of ABT models on a vertical array.

4.1. P-SV wave seismic response

The simulated horizontal component of P-SV wave seismic response of elastic ABTM1 model on a vertical array along the axis of ABT is shown in Fig. 7a. An analysis of Fig. 7a depicts the direct diffracted P-wave at the corners, transmitted SV-wave, reflected-transmitted-mode converted P-wave, reflected-trans-

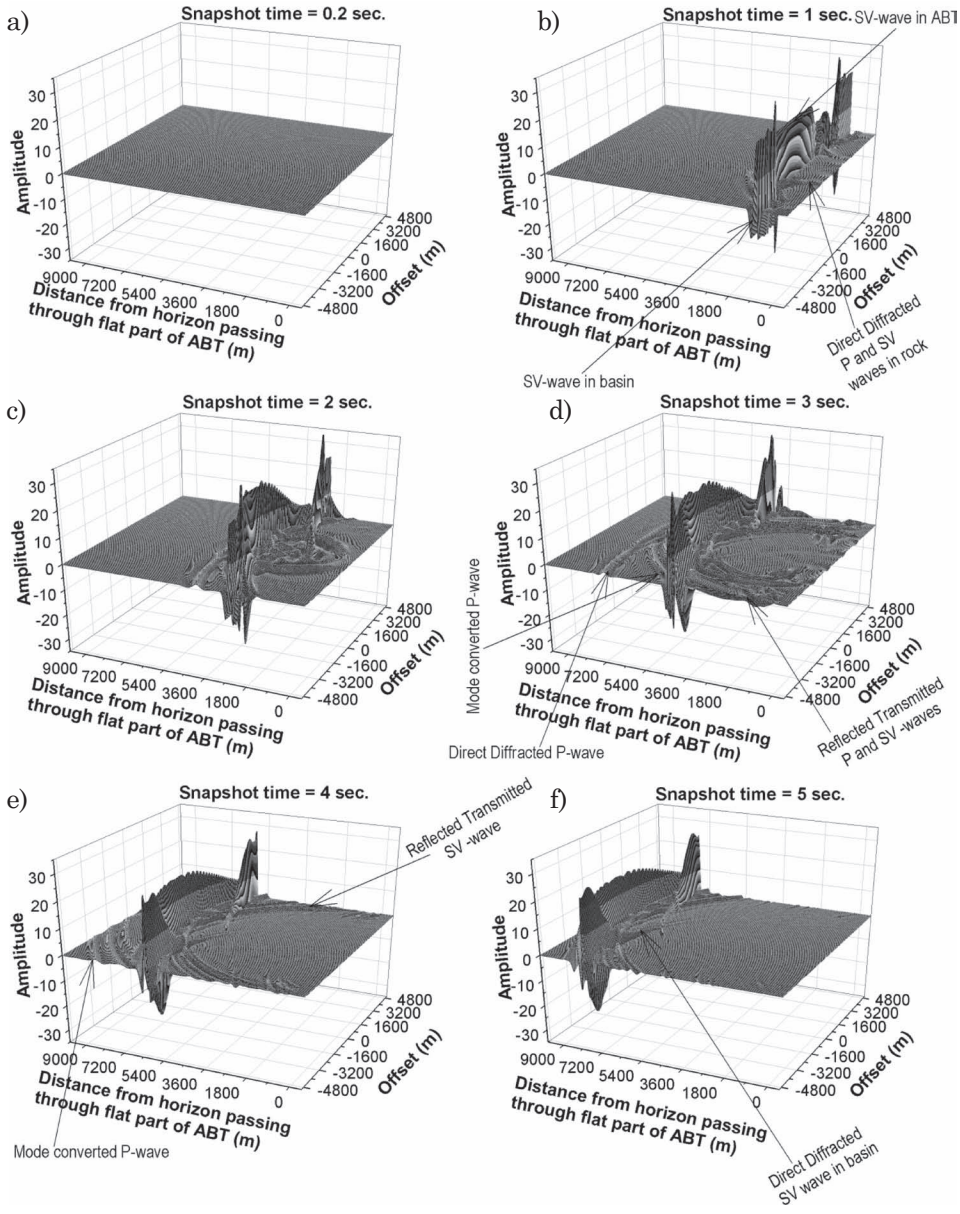

Figure 8. Snapshots of horizontal component of P-SV wave in a rectangular area at different times.

mitted SV-wave (reflected SV-wave from inner part of ABT and then transmitted in to basin as mode converted P-wave also) and direct-diffracted SV-wave at the corners are the first, second, third, fourth and fifth arrivals, respectively. There

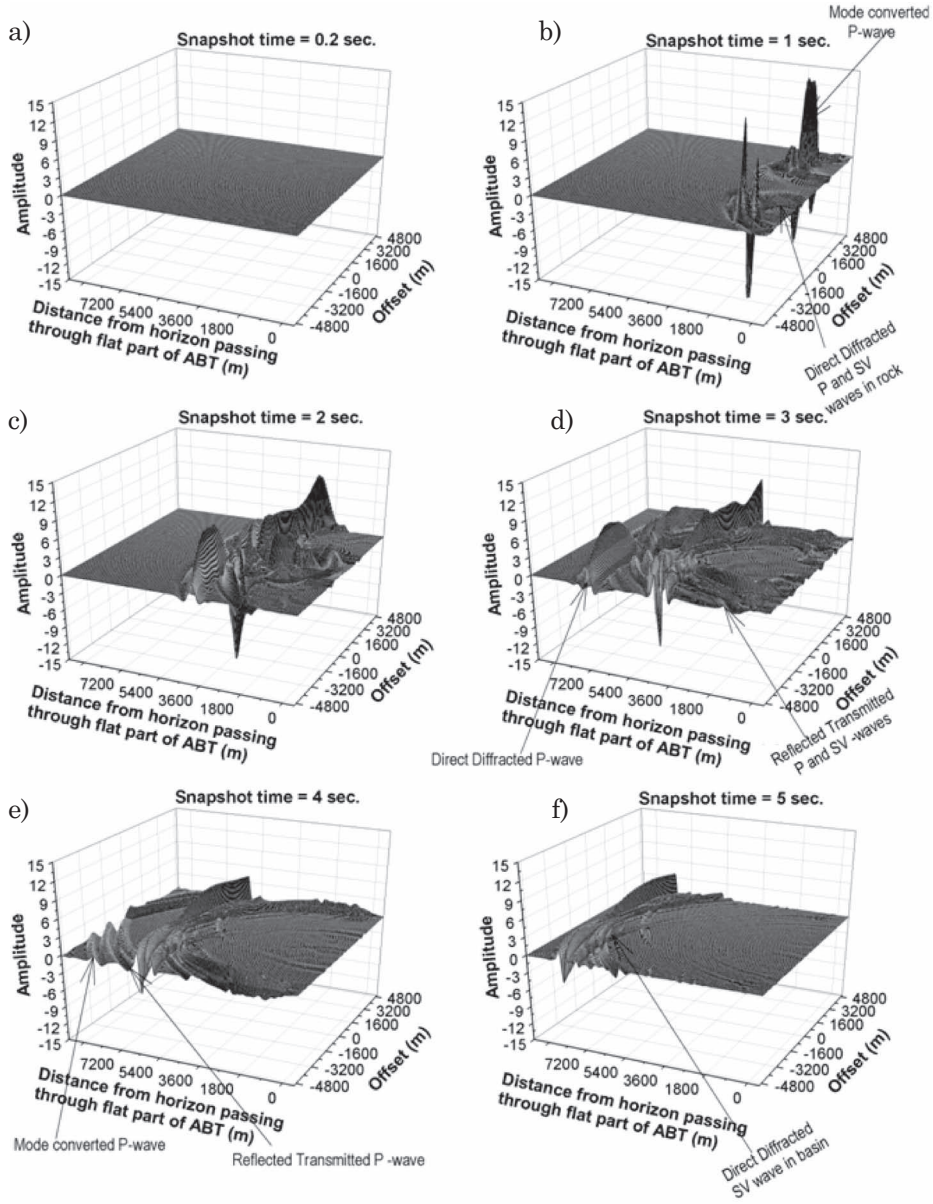

Figure 9. Snapshots of vertical component of P-SV wave in a rectangular area at different times.

is decrease of amplitude of transmitted SV-wave with increase of distance travelled in basin due to the ABT de-focusing effect. The amplitudes of diffracted waves are highly variable. The receiver R1 located in basement depicts both the

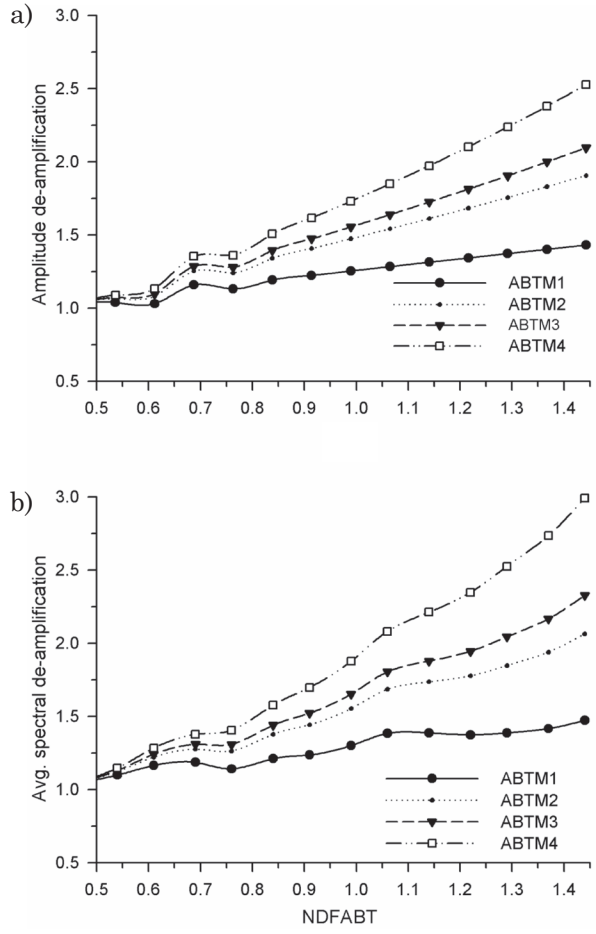

Figure 10. Amplitude de-amplification factor (a) and average spectral de-amplification factor at different NDFABT values (b).

up-going and the reflected SV-waves from the ABT. Similarly, Figs. 7b–7d show the responses of viscoelastic ABTM2-ABTM4 models, respectively. The analysis of Fig. 7 reveals the effects of rheology on the decrease of amplitudes of the transmitted, reflected-transmitted, mode converted and the diffracted waves in accordance with the sediment damping.

4.2. P-SV wave snapshots

P-SV wave snapshots were also computed in the same rectangular area as that for SH-wave. Figs. 8 and 9 show the snapshots of horizontal and vertical

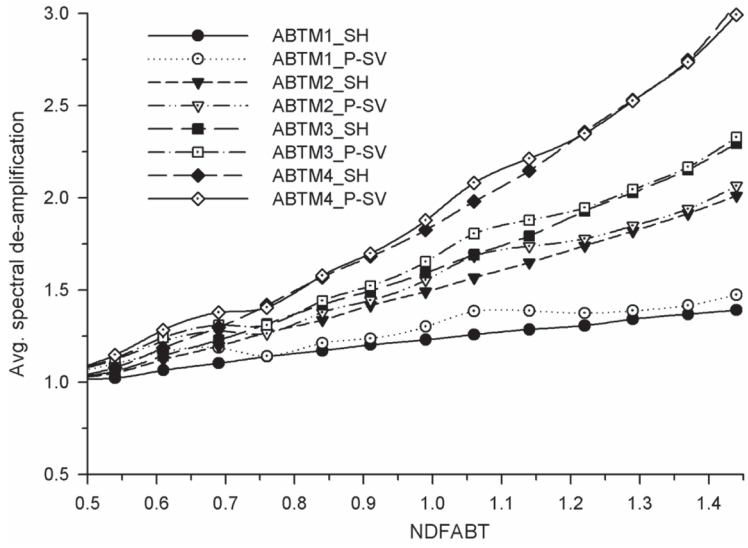

Figure 11. Comparison of de-amplification factors for SH-wave and SV-wave along the focal length of ABT.

components at different times. Fig. 8b shows the SV-wave entered into the anticlinal part of ABT, direct-diffracted waves from the corners of ABT and transmitting SV-wave in basin along the horizontal flanks of the ABT. The intense mode converted P-wave and direct-diffracted P- and SV-waves can be seen in Fig. 9b at snapshot time 1.0 sec. The focusing of reflected P- and SV-waves from the curved inner part of ABT and splitting of main SV-wave front can be inferred in snapshots at time 2.0 second (Figs. 8c and 9c). The reflected-transmitted SV-wave, diffracted P-wave and mode converted P-wave and the transmitted SV-wave in sediment can be seen in snapshot at time 3.0 second in both the components (Figs. 8d and 9d). The snapshots of horizontal and vertical components at time 4.0 sec (Figs. 8e and 9e) depicts mode converted and reflected-transmitted P-waves, reflected-transmitted SV-wave, direct-diffracted SV-wave, reflected-diffracted SV-wave in the basin. The analysis of Figs. 8 and 9 reveals the decrease of amplitude of transmitted SV-wave along the axis of ABT due to de-focusing.

4.3. P-SV wave spectral de-amplification

The computed amplitude de-amplification factor and average spectral de-amplification factor at different NDFABT positions are shown in Fig. 10. There is an increase of both the amplitude de-amplification factor and average spectral de-amplification factors with the increase of NDFABT value and the sediment damping. It is somewhat larger in the later one, especially in case of larger sediment damping. A comparison of average spectral de-amplification factors for

SH- and SV-waves for different sediment damping is shown in Fig. 11. This figure depicts good similarity in average spectral de-amplification at different NDFABT positions for different sediment damping. The de-amplification factors are somewhat larger in SV-wave case which may be attributed to the intense mode conversion of SV-wave at the lower part of flanks of ABT. But, the intense mode conversion of SV-wave has not affected the de-focusing effects along the axis of ABT to the level as expected. Mode conversion may affect the ground motion spatially in horizontal direction.

5. Discussion and conclusions

A very peculiar damage pattern was observed in Santa Monica, Los Angeles basin during Northridge earthquake of 1994 (Gao et al., 1996; Alex and Olsen, 1998; Davis et al., 2000) and consistent anomalous damage to unreinforced brick chimneys in west Seattle, Washington during 1949 Olympia earthquake, 1965 Tacoma earthquake and 2001 Nisqually earthquake (Booth et al., 2004; Stephenson et al., 2006) due to the basement focusing effects. It means, during earthquakes there may be certain localities where anomalously lesser damage may occur due to basement de-focusing effects. Such observations are not reported after earthquakes because of less or no damage to buildings, although may be noticed. Further, no theoretical study related to ABT de-focusing effects is available in the literature. In order to fulfill this gap as well as to find out the level of de-amplification caused by ABT, this study was carried out.

The snapshots along with the simulated responses of ABT models for different rheology of sediment revealed ABT de-focusing effects, generation of mode converted waves from the curved part of ABT and diffracted waves from the corners of the ABT. It can be concluded that in-plane de-focusing effects along the focal length are more or less similar to the out of plane de-focusing although there was intense mode conversion of incident SV-wave at the lower part of flanks of ABT. Elastic response of the model revealed that the de-amplification caused by ABT was not frequency dependent in contrast to the basement focusing which causes frequency dependent spectral amplification (Davis et al., 2000; Narayan and Kumar, 2012, 2013). An increase of spectral de-amplification factor with the increase of frequency and distance from the tip of ABT was inferred in accordance with the sediment damping and distance. The basement de-focusing may cause 20–30% reduction of amplitude (excluding the sediment damping) depending on the depth of basement. The findings of this research work reveal that a detailed study of basement de-focusing is necessary for seismic hazard assessment and cost effective earthquake engineering.

Acknowledgements – Authors are grateful to the reviewer for his insightful comments and suggestions which significantly improved the revised manuscript. The second author is also grateful to the Ministry of Earth Sciences, New Delhi and Council of Scientific and Industrial Research, New Delhi for financial assistance through Grant Numbers MES-484-EQD and CSR-569-EQD, respectively.

References

Alex, C. M. and Olsen, K. B. (1998): Lens-effect in Santa Monica?, *Geophys. Res. Lett.*, **25**, 3441– 3444.

Booth, D. B., Wells, R. E. and Givler, R. W. (2004): Chimney damage in the greater Seattle area from the Nisqually earthquake of 28 February 2001, *B. Seismol. Soc. Am.*, **94**, 1143–1158.

Clayton, R. W. and Engquist, B. (1977): Absorbing boundary conditions for acoustic and elastic wave equations, *B. Seismol. Soc. Am.*, **67**, 1529–1540.

Day, S. M. and Minster, J. B. (1984): Numerical simulation of wavefields using a Padé approximant method, *Geophys. J. Roy. Astr. Soc.*, **78**, 105–118.

Davis, P. M., Justin, L., Rubinstein, K. H., Liu, S. S. and Knopoff, G. L. (2000): Northridge earthquake damage caused by geologic focusing of seismic waves, *Science*, **289**, 1746–**1750.**

Emmerich, H. and Korn, M. (1987): Incorporation of attenuation into time-domain computations of seismic wave fields, *Geophysics*, **52**, 1252–1264.

Gao, S., Liu, H., Davis, P. M. and Knopoff, G. L. (1996): Localized amplification of seismic waves and correlation with damage due to the Northridge earthquake, *B. Seismol. Soc. Am.*, **86**, S209–230.

Israeli, M. and Orszag, S. A. (1981): Approximation of radiation boundary conditions, *J. Comp. Phys.*, **41**, 115–135.

Kristeck, J. and Moczo, P. (2003): Seismic wave propagation in viscoelastic media with material disconuties – a 3D 4th order staggered grid finite difference modeling, *B. Seismol. Soc. Am.*, **93**, 2273–2280.

Kumar, S. and Narayan, J. P. (2008): Implementation of absorbing boundary conditions in a 4th order accurate SH-wave staggered grid finite difference algorithm with variable grid size, *Acta Geophys.*, **56**, 1090–1108.

Levander, A. R. (1988): Fourth-order finite-difference P-SV seismograms, *Geophysics*, **53**, 1425–1436.

Madariaga, R. (1976): Dynamics of an expanding circular fault. *B. Seismol. Soc. Am.*, **67**, 163–182.

Moczo, P., Kristek, J., Vavrycuk, V., Archuleta, R. J. and Halada, L. (2002): 3D heterogeneous staggered-grid finite-difference modelling of seismic motion with volume harmonic and arithmetic averaging of elastic moduli and densities, *B. Seismol. Soc. Am.*, **92**, 3042–3066.

Narayan, J. P. (2003): 2.5D simulation of ridge-weathering effects on the ground motion characteristics, *J. Earthq. Eng.*, **7**, 447–461.

Narayan, J. P. and Rao Prasad, P. V. (2003): Two and half dimensional simulation of ridge effects on the ground motion characteristics, *Pure Appl. Geophys.*, **160**, 1557–1571.

Narayan, J. P. (2005): Study of basin-edge effects on the ground motion characteristics using 2.5-D modeling, *Pure Appl. Geophys.*, **162**, 273–289.

Narayan, J. P. and Ram, A. (2006): Study of effects of underground ridge on the ground motion characteristics, *Geophys. J. Int.*, **165**, 180–196.

Narayan, J. P. and Kumar, S. (2008): A 4th order accurate SH-wave staggered grid finite-difference algorithm with variable grid size and VGR-stress imaging technique, *Pure Appl. Geophys.*, **165**, 271–294.

Narayan, J. P. and Kumar, S. (2010): A 4th order accurate P-SV wave staggered grid finite difference algorithm with variable grid size and VGR-stress imaging technique, *Geofizika*, **27**, 45–68.

Narayan, J. P. (2012): Effects of P-wave and S-wave impedance contrast on the characteristics of basin transduced Rayleigh waves, *Pure Appl. Geophys.*, **169**, 693–709.

Narayan, J. P. and Kumar, V. (2012): Numerical study of effects of synclinal basement topography on ground motion characteristics (Paper No. 3144), in *Proceedings of the 15th World Conference on Earthquake Engineering (15WCEE)*, Lisbon, Portugal, September 24–28.

Narayan, J. P. and Kumar, V. (2013): P-SV wave time-domain finite-difference algorithm with realistic damping and a combined study of effects of sediment rheology and basement focusing, *Acta Geophys.* (Revised version submitted).

Stephenson, W. J., Frankel, A. D., Odum, J. K., Williams, R. A. and Pratt, T. L. (2006): Toward resolving an earthquake ground motion mystery in west Seattle, Washington State: Shallow seismic focusing may cause anomalous chimney damage, *Geophys. Res. Lett.*, **33**, L06316, DOI: 10.1029/2005GL025037.

SAŽETAK

Utjecaj sedimentne reologije i antiklinalne bazenske topografije na karakteristike gibanja tla

Vinay Kumar i J. P. Narayan

Fokusiranje potresnih valova topografijom pripadnih strukturnih bazena uzrokovalo je neobičnu razdiobu šteta koja je opažena nakon potresa u Northridgeu 1994. i Nisqualliyu 2001. godine. U skladu s time moguće je očekivati i defokusiranje valova potresa antiklinalnom bazenskom topografijom (ABT), ali, koliko nam je poznato, do sada nije objavljena niti jedna studija koja bi se bavila tim problemom. Kako bismo ispunili tu prazninu, ovdje smo razmotrili kombinirani utjecaj reologije sedimenata i ABT na svojstva SH i SV-valova. Rezultati simulacije ukazuju na povećanje deamplifikacije s udaljenosti koju valovi prevale u bazenu iznad ABT. Sintetizirani seizmogrami također potvrđuju deamplifikaciju amplituda, difrakciju te konverziju modova u slučaju SV-valova. Deamplifikacija ne ovisi o frekvenciji. Prosječni spektralni faktori deamplifikacije su gotovo jednaki za obje vrste valova, čak i nakon jake konverzije SV-valova u donjim dijelovima ABT. Na temelju simulacija zaključeno je da su efekti ABT u procjeni potresne opasnosti za učinkovito porotupotresno projektiranje jednako važni kao i efekti sinklinalne topografije (SBT).

Ključne riječi: simulacije viskoelastičnog seizmičkog odziva, metoda konačnih razlika, konverzija modova, efekt bazenske topografije, efekti lokalnog tla

Corresponding authors' address: Vinay Kumar and J. P. Narayan, Indian Institute of Technology Roorkee, Department of Earthquake Engineering, Roorkee-247667, India; e-mail: jaypnfeq@iitr.ernet.in